Title	Natural convection heat transfer from horizontal rod bundles in liquid sodium. Part 2: Correlations for horizontal rod bundles based on theoretical results
Author(s)	Hata, Koichi; Takeuchi, Yuto; Hama, Katsuhiko; Shiotsu, Masahiro
Citation	Journal of Nuclear Science and Technology (2014), 52(3): 342-354
Issue Date	2014-08-13
URL	http://hdl.handle.net/2433/198283
Right	The Version of Record of this manuscript has been published and is available in Journal of Nuclear Science and Technology (2014) http://www.tandfonline.com/10.1080/00223131.2014.947347.; 2015-08-13 .
Type	Journal Article
Textversion	author

Natural convection heat transfer from horizontal Rod bundles in liquid sodium

Part 2 : Correlations for horizontal rod bundles based on theoretical results

Koichi Hata[a]*, Yuto Takeuchi[a], Katsuhiko Hama[b] and Masahiro Shiotsu[b]

[a] *Institute of Advanced Energy, Kyoto University, Gokasho, Uji, Kyoto 611-0011, Japan*

[b] *Dept. of Energy Science and Technology, Kyoto University, Sakyo-ku, Kyoto 606-8501, Japan*

Natural convection heat transfer from horizontal rod bundles in $N_{xm} \times N_{ym}$ arrays (N_{xm}, N_{ym}=5~9) in liquid sodium was numerically analyzed for three types of the bundle geometry (in-line rows, staggered rows I and II). The unsteady laminar two dimensional basic equations for natural convection heat transfer caused by a step heat flux were numerically solved until the solution reaches a steady-state. The PHOENICS code was used for the calculation considering the temperature dependence of thermo-physical properties concerned. The surface heat fluxes for each cylinder were equally given for a modified Rayleigh number, R_f, ranging from 0.0637 to 63.1 (q=1×10⁴~7×10⁶ W/m²). S_x/D and S_y/D for the rod bundle, which are ratio of the distance between center axes on the abscissa and the ordinate to the rod diameter, were ranged from 1.6 to 2.5 on each bundle geometry. The spatial distribution of Nusselt numbers, Nu, on horizontal rods of a bundle was clarified. The average value of Nusselt number, Nu_{av}, for three types of the bundle geometry with various values of S_x/D and S_y/D were calculated to examine the effect of the array size, S/D and R_f on heat transfer. The bundle geometry for the higher Nu_{av} value under the condition of $S_x/D \times S_y/D$=4 was examined by changing the ratio of S_x/S_y. A correlation for Nu_{av} for three types of bundle geometry above mentioned including the effects of S_x/D and S_y/D was developed. The correlation can describe the theoretical values of Nu_{av} for three types of the bundle geometry in $N_{xm} \times N_{ym}$ arrays (N_{xm},

N_{ym}=5~9) for S_x/D and S_y/D ranging from 1.6 to 2.5 within 10 % difference.

Key words ; natural convection heat transfer; liquid sodium; horizontal rod bundle

[*]Corresponding author. Email: hata@iae.kyoto-u.ac.jp

1. Introduction

Knowledge of natural convection heat transfer from a horizontal rod bundle in liquid sodium is important as a database for the design of a heat exchanger in a fast breeder reactor for decay heat removal at a loss of flow accident. However, there have been little fundamental experimental work in liquid sodium and little is known on the effects of bundle geometry and value of *S/D* (ratio of the distance between center axes, *S*, to the rod diameter, *D*) on heat transfer.

There have been a few works on interactions between two or more horizontal cylinders in natural convection. Marsters [1] carried out a study of three, five and nine horizontal cylinders in a vertical array in air. They have found that for closely spaced arrays, individual tube Nusselt numbers are smaller than for a single cylinder, and for wide spacing individual tube Nusselt numbers are higher than for a single cylinder. Lieberman and Gebhard [2] have conducted experiments in air on the interactions of heated wires arranged in a plane array. The array could be oriented so that its plane made angles of 0°, 30°, 60° and 90° with the vertical. Their data were for the wire spacing ranging from 37.5 diameters to 225 diameters.

Correlations for natural convection heat transfer from 4 to 16 horizontal cylinders to cubical enclosures were represented by Warrington and Weaver [3], but the effect of cylinder geometry on heat transfer and the heat transfer coefficients on each cylinder were not discussed. Natural convection heat transfer experiments on horizontal rod bundle for design of casks for transportation, storage, and permanent disposal of spent nuclear assemblies have been conducted with air and helium in enclosing cask by Fedorovitch [4], Irino et al. [5], and Vdovets et al. [6].

Keyhani and Luo [7] carried out numerical simulations with air and helium in 3×3 to 9×9 arrays, predicted the average Nusselt number of each rod for a modified Rayleigh number, $Ra_d{}^*$, of 1 to 3.16×10^2 and obtained pure conduction results for rod bundles ranging 3×3 to 13×13 arrays.

Keyhani and Dalton [8] experimentally investigated natural convection heat transfer in enclosed $N{\times}N$ arrays (N=3, 5 and 7) of electrically heated rods and correlated a generalized enclosure Nusselt number as a function of enclosure modified Rayleigh number and the array size (N).

In Part 1 of this paper, the natural convection heat transfer coefficients on two parallel horizontal cylinders have already been obtained experimentally and theoretically for various setting angles, γ, between the vertical direction and the plane including both of these center axes, over the range of zero to 90° in liquid sodium and the correlations for two cylinders were presented as a function of R_f [$=Gr^*Pr^2/(4+9Pr^{1/2}+10Pr)$], S/D and γ based on theoretical solutions. The theoretical values of average Nusselt number, Nu, on each of these two cylinders are in agreement with the corresponding experimental data with the deviations less than 15 %. A combined correlation for multi-cylinders in a vertical array was presented based on the correlations for two cylinders. The average Nusselt numbers on each of the cylinders predicted by the correlation were in agreement with the corresponding theoretical solutions for R_f ranging from 4.7 to 63 within 10 % difference.

The objectives of present study are: (1) to obtain the numerical solutions of the average Nusselt number from theoretical laminar natural convection equations for a wide range of the array size ($N_{xm}{\times}N_{ym}$), S/D and R_f on three bundle geometries (in-line rows, staggered rows I and II), (2) to clarify the effect of the array size, S/D, R_f and the bundle geometry on heat transfer, (3) to obtain the bundle geometry accompanied with a higher heat transfer coefficient, and (4) to present a correlation to describe the effect of the array size, S/D, R_f and the bundle geometry on natural convection heat transfer.

2. Theoretical Solution of Laminar Natural Convection Equations

2.1 Fundamental Equations

Considering the one-half symmetry of the problem, the unsteady laminar two

dimensional basic equations in boundary fitted coordinates as shown in **Figures 1 (a) and (b)**

for a 5×5 array are described as follows.

(Continuity Equation)

$$\frac{\partial \rho}{\partial t} + \frac{\partial}{\partial x}(\rho u) + \frac{\partial}{\partial y}(\rho v) = 0 \tag{1}$$

(Momentum Equation)

$$\frac{\partial}{\partial t}(\rho u) + \frac{\partial}{\partial x}(\rho u u) + \frac{\partial}{\partial y}(\rho v u) = -\frac{\partial P}{\partial x} + \frac{\partial}{\partial x}\tau_{xx} + \frac{\partial}{\partial y}\tau_{xy} \tag{2}$$

$$\frac{\partial}{\partial t}(\rho v) + \frac{\partial}{\partial x}(\rho u v) + \frac{\partial}{\partial y}(\rho v v) = -\frac{\partial P}{\partial y} + \frac{\partial}{\partial x}\tau_{yx} + \frac{\partial}{\partial y}\tau_{yy} - \rho g \tag{3}$$

(Energy Equation)

$$\frac{\partial}{\partial t}(\rho c_p T) + \frac{\partial}{\partial x}(\rho c_p u T) + \frac{\partial}{\partial y}(\rho c_p v T) = \frac{\partial}{\partial x}\{\frac{\lambda}{c_p}\frac{\partial}{\partial x}(c_p T)\} + \frac{\partial}{\partial y}\{\frac{\lambda}{c_p}\frac{\partial}{\partial y}(c_p T)\} \tag{4}$$

where

$$\tau_{xx} = 2\rho v \frac{\partial u}{\partial x}, \quad \tau_{yy} = 2\rho v \frac{\partial v}{\partial y}, \quad \tau_{xy} = \tau_{yx} = \rho v\left(\frac{\partial u}{\partial y} + \frac{\partial v}{\partial x}\right) \tag{5}$$

u, v are the *x, y* components of a velocity vector, respectively.

< Figure 1 (a) and (b) >

2.2 Boundary Conditions

The fundamental equations are numerically analyzed together with the following

boundary conditions.

On the surfaces of cylinders: constant heat flux, and non-slip condition.

At the right outer boundary:

$$T = T_0, \quad \frac{\partial u}{\partial x} = 0 \text{ for in-flow,}$$

$$\frac{\partial T}{\partial x} = 0, \quad \frac{\partial u}{\partial x} = 0 \text{ for out-flow.}$$

At the lower and upper boundary:

$$T = T_0, \quad \frac{\partial v}{\partial y} = 0 \text{ for in-flow,}$$

$$\frac{\partial T}{\partial y} = 0, \quad \frac{\partial v}{\partial y} = 0 \text{ for out-flow.}$$

where T_0 is a bulk liquid temperature.

2.3 Method of Solution

The control volume discretization equations were derived from these fundamental equations by using the hybrid scheme [9]. The thermo-physical properties for each control volume are given as those at each volume temperature. The procedure for the calculation of the flow field is the SIMPLE algorithm which stands for Semi-Implicit Method for Pressure-Linked Equations.

The surface heat fluxes, q, for each cylinder were equally given in the range of 1×10^4 W/m^2 to 7×10^6 W/m^2 as an initial condition, and numerical calculation was continued until the steady-state was obtained. The surface temperature on the cylinder was calculated from the analyzed temperature of the first control volume on the cylinder surface, *TEM*, which is supposed to be located on the center of the control volume, by solving the thermal conduction equation in liquid sodium as follows [10-14].

$$T_s = \frac{q}{\lambda_l} \frac{(\Delta r)_{out}}{2} + TEM \tag{6}$$

where, $(\Delta r)_{out}$ is the outer control volume width for the *r*-component. The liquid temperatures on the test tube surface in the conductive sub-layer [15, 16] will become linearly lower with

an increase in the radius by the heat conduction from the surface temperature on the test tube, $T_f=T_s-\Delta rq/\lambda_l$. And let those, T_f, equal the analyzed liquid temperature of the outer control volume on the test tube surface, *TEM*, as given in Eq. (6). Half the outer control volume width for the r-component, $(\Delta r)_{out}/2$, would become the thickness of the conductive sub-layer for the local heat transfer in a horizontal cylinder under two-phase model classified into laminar sub-layer and transition region of the buoyancy-driven flow. Average heat transfer coefficient on the cylinder surface was obtained by averaging the calculated local surface temperatures at every 10° in θ. All the calculations were made by using the PHOENICS code [17].

3. Results and Discussion

In this section, correlations of natural convection heat transfer for a single horizontal cylinder and two horizontal cylinders, and a combined correlation for multi-cylinders in a vertical array previously obtained are firstly explained. The correlation from horizontal rod bundles of in-line rows and staggered rows I and II in $N_{xm} \times N_{ym}$ arrays is presented by use of these correlations.

3.1 The Correlations Previously Obtained

3.1.1 For a Single Horizontal Cylinder

The following correlation for *Nu* was given as a function of R_f by least square fitting within ± 4 % .

$$\mathrm{Nu} = 10^z \tag{7}$$

where

$$z = 0.193385 + 0.145037 \ \log \mathrm{R}_f + 0.664323 \times 10^{-2} (\log \mathrm{R}_f)^2$$
$$- 0.232432 \times 10^{-3} (\log \mathrm{R}_f)^3 - 0.238613 \times 10^{-4} (\log \mathrm{R}_f)^4$$

In this work, Nusselt numbers on horizontal rods of a bundle and their average value obtained theoretically for a wide range of surface heat flux are compared with those given by

7

Equation (7) at the same condition.

3.1.2 For Two Horizontal Cylinders

The calculated values of Nu/Nu_{SC} for the upper and lower cylinders were approximately expressed by the following correlations.

For the upper cylinder:

$$Nu / Nu_{SC} = 1 - 0.60 \exp[-AR_f^m (S/D)] \tag{8}$$

where $A = 0.29 + 6.8 \times 10^{-3} \gamma$, $m = 0.12 + 1.67 \times 10^{-3} \gamma$

For the lower cylinder:

$$Nu / Nu_{SC} = 1 - C \exp[-KR_f^n (S/D)] \tag{9}$$

where

$$\begin{aligned}
&C = 0.4 + 2.2 \times 10^{-3} \gamma, \\
&K = 0.56 + 0.34(S/D)\sin\gamma && : \quad 0 \le \gamma \le arcsin(D/S), \\
&K = 0.9 && : \quad \gamma > arcsin(D/S), \\
&n = 0.16 + 1.2 \times 10^{-3} \gamma.
\end{aligned}$$

The values of Nu/Nu_{SC} derived from these correlations were in agreement with the numerical solutions for the upper and lower cylinders within -5 and +9 % error.

3.1.3 For Multi-cylinders in a Vertical Array

A combined correlation for multi-cylinders in a vertical array with a constant S/D was given based on the correlations for two cylinders in Part 1 of this work. Each horizontal cylinder consisting the vertical array were numbered sequentially from $i=1$ (lowermost cylinder) to $i=N_m$ (uppermost one). The combined correlation was as follows:

$$\begin{aligned}
\left[Nu / Nu_{SC} \right]_{i=a} &= \prod_{i=1}^{a-1} [1 - 0.60 \exp\{-AR_f^m (a-i)S/D\}] \\
&\times \prod_{i=a}^{N_m -1} [1 - C \exp\{-KR_f^n (N_m -i)S/D\}]
\end{aligned} \tag{10}$$

where the Nu/Nu_{SC} value for a cylinder with $i=a$ was given by multiplying the mutual effects between the cylinder and other lower and upper cylinders.

3.2 Calculated Results for Horizontal Rod Bundles of In-line Rows for $S_x=S_y$

Natural convection heat transfer from horizontal rod bundles in $N_{xm} \times N_{ym}$ arrays was numerically analyzed for the bundle geometry of in-line rows (IR) as shown in **Figure 2 (a)**. S_x/D and S_y/D for the rod bundle which are ratios of the distance between center axes on the abscissa and the ordinate to the rod diameter were ranged from 1.6 to 2.5 in 5×5, 7×7 and 9×9 arrays. The surface heat fluxes for each cylinder were equally given at 1×10^4, 2×10^4, 7×10^4, 2×10^5, 7×10^5, 1×10^6, 2×10^6 and 7×10^6 W/m². The parameters used for the calculation are tabulated in **Table 1**.

< Figure 2 (a), (b) and (c) >

< Table 1 >

The numerical results of *Nu* on a rod bundle of a 5×5 array with $S_x/D=S_y/D=2$ for $R_f=1.30$ and 6.79 ($q=2\times10^5$, 1×10^6 W/m²) were shown in **Figures 3 and 4** as typical examples. They are shown as the ratio of *Nu* to those for a single cylinder given by Equation (7) for the same condition, Nu/Nu_{SC}, versus N_x graph with N_y as a parameter, where N_x is the column number and N_y is the row number (N_x=1, 5 are the edge columns; N_x=3 is the center column; N_y=1 is the lowest row; N_y=5 is the uppermost row). The values of Nu/Nu_{SC} are symmetrical on the graph. The value of Nu/Nu_{SC} on each column for N_y=1 (the lowest row) is higher than those for other rows. The value at N_x=3 for N_y=1 is the maximum. The values of Nu/Nu_{SC} for each column become smaller with the increase in the row number. The Nu/Nu_{SC} value at N_x=3 for N_y=5 is the minimum. The values of Nu/Nu_{SC} at N_x=1, 5 (edge column) are higher than those for other columns on the same row number except those for N_y=1.

< Figure 3 and 4 >

The contour of liquid temperature and the distribution of velocity vectors on a rod bundle of a 5×5 array for $R_f=6.79$ were plotted in **Figures 5 and 6**, respectively. It is recognized that a flow of liquid sodium turns to the center column and ascends along it. The liquid temperature on the edge column and the lowest row is lower and that on the center column

becomes higher with the increase in the row number as mentioned above.

< Figure 5 and 6 >

The values of Nu/Nu_{SC} are also shown versus N_y with N_x as a parameter in **Figures 7 and 8**. The values of Nu/Nu_{SC} for N_x=1,5 (edge column) are far higher than those for other column except the lowest row (N_y=1). The edge column are not affected by the thermal boundary layer from the lower cylinder, because of being a in-flow plane. The values of Nu/Nu_{SC} for N_x=2,4 are almost in agreement with those for N_x=3 (center column), the values for N_x=3 are about 8 % higher and about 13 % lower than those for N_x=2,4 at the lowest row and the uppermost row, respectively. The values of Nu/Nu_{SC} for each rod derived from the combined correlation in a vertical array, Equation (10), are shown as a solid curve in each figure for comparison. The value at N_y=1 for N_x=3 is higher than the curve of the combined correlation, because of the contribution of the fluid flow caused by the buoyancy force, and the value at N_y=5 for N_x=3 is lower than the curve, because of the development of the thermal boundary layer by the mutual effects between the center rod and other surrounding rods. It is shown from these figures that the values of Nu/Nu_{SC} on the same column and row numbers become smaller with the decrease in R_f.

< Figure 7 and 8 >

As shown in **Figures 7 and 8**, the value of Nu on the center column shows the same trend of dependence as predicted by the combined correlation in a vertical array, but that on the edge column is far higher than the corresponding value. The average value of the Nusselt numbers for the rods in the bundle was obtained to develop the correlation for the rod bundle and to discuss the effect of the array size and the bundle geometry on the heat transfer. The average Nusselt number, Nu_{av}, for a rod bundle in $N_{xm} \times N_{ym}$ array was obtained as follows,

$$Nu_{av} = \sum_{i=1}^{N_{xm}} \sum_{j=1}^{N_{ym}} Nu_{ij} / (N_{xm} \times N_{ym}) \tag{11}$$

where Nu_{ij} is the Nusselt number for i-th column and j-th row.

10

The ratios of Nu_{av} to those for a single cylinder given by Equation (7) at the same condition, Nu_{av}/Nu_{SC}, for the rod bundle in a 5×5 array with $S_x/D=S_y/D=2$ are plotted on the Nu_{av}/Nu_{SC} versus R_f graph in **Figure 9** for R_f ranging from 0.064 to 63.1 ($q=1\times10^4\sim7\times10^6$ W/m²). The Nu_{av}/Nu_{SC} values are 34 % of a single cylinder at $R_f=0.0637$ ($q=1\times10^4$ W/m²), 80 % at $R_f=14.2$ ($q=2\times10^6$ W/m²) and 87 % at $R_f=63.1$ ($q=7\times10^6$ W/m²): they increase with the increase in R_f and approach asymptotically the value of a single cylinder. It is suggested that the Nu_{av} values for the rod bundle are smaller than those for a single cylinder in the lower heat flux region because convection heat transfer is small and the thermal boundary layer becomes thicker for interactions between one rod and the others due to the effect of thermal conduction.

< Figure 9 >

It is assumed that the Nu_{av} may be proportional to the average value of the Nusselt numbers on the center column, $(Nu_{CC})_{av}$. The values of Nu_{av}/Nu_{SC} in a 5×5 array are shown versus $(Nu_{CC})_{av}/Nu_{SC}$ in **Figure 10**, where $(Nu_{CC})_{av} = \sum\limits_{j=1}^{N_{ym}} Nu_{center-column,j} / N_{ym}$. The theoretical values of Nu_{av}/Nu_{SC} on the center column for rod bundles in 7×7 and 9×9 arrays with $S_x/D=S_y/D=2$ are also shown in this figure. They are approximately expressed by a single curve given by the following equation.

$$Nu_{av} / Nu_{SC} = 1.18\,(Nu_{CC})_{av} / Nu_{SC} \tag{12}$$

< Figure 10 >

It is further assumed that $(Nu_{CC})_{av}$ may be expressed as a function of the average value of the Nusselt numbers on a single vertical array, $(Nu_{SB})_{av}$. The $(Nu_{CC})_{av}/Nu_{SC}$ values on the center column for the rod bundles in 5×5, 7×7 and 9×9 arrays are shown versus the corresponding values of $(Nu_{SB})_{av}/Nu_{SC}$ in **Figure 11**, where $(Nu_{SB})_{av} / Nu_{SC} = \sum\limits_{i=1}^{N_m} [Nu / Nu_{SC}]_i / N_m$ derived from Equation (10), $N_m = N_{ym}$ and

$S = S_y$. As shown in the figure, they are approximately expressed by the following equation.

$$\left(Nu_{CC}\right)_{av} / Nu_{SC} = 1.5\left(Nu_{SB}\right)_{av} / Nu_{SC} - 0.738 / \left(N_{xm} \times N_{ym}\right)^{1/4} \tag{13}$$

Combining Equations (12) and (13) leads to,

$$Nu_{av} / Nu_{SC} = 1.77\left(Nu_{SB}\right)_{av} / Nu_{SC} - 0.871 / \left(N_{xm} \times N_{ym}\right)^{1/4} \tag{14}$$

The values of Nu_{av}/Nu_{SC} derived from Equation (14) for rod bundles in 5×5, 7×7 and 9×9 arrays with $S_x/D=S_y/D=2$ are compared with the corresponding numerical solutions in **Figures 9, 12 and 13**, respectively. The theoretical solutions of Nu_{av}/Nu_{SC} for R_f ranging from 0.0637 to 63.1 are expressed by Equation (14) within a few % difference.

< Figure 11, 12 and 13 >

3.3 Effect of the Bundle Geometry on Heat Transfer

Natural convection heat transfer for rod bundles in 5×5 and 5(6)×5 arrays was numerically analyzed on two types of staggered rows I and II (SRI and SRII) for $S_x/D=S_y/D=2$ at R_f=4.67, 6.78 and 14.2 (q=7×10^5, 1×10^6, 2×10^6 W/m^2). Schematics for the bundle geometry of staggered rows I and II are shown in **Figures 2 (b) and (c)**. In case of staggered rows, unit volume is a triangle and S_x and S_y are defined as shown in these figures. The rod bundle of staggered rows II in a 5(6)×5 array shown in **Figure 2 (c)** has 6 rods at an even number of rows in the array because the entire rod bundle is symmetric with respect to the y axis, and has 27 rods (5×5+2) in all. S_x and S_y are the distance between center axes on the abscissa and the ordinate as shown in the figures. The values of Nu_{av}/Nu_{SC} for two types of staggered rows I and II with $S_x/D=S_y/D=2$ are shown versus the rod bundle geometries with R_f as a parameter in **Figure 14** with those for in-line rows (IR). The Nu_{av}/Nu_{SC} values for each bundle geometry are higher for higher R_f. The values of Nu_{av}/Nu_{SC} for two types of staggered rows I and II are in good agreement with those of in-line rows.

And, the values of Nu_{av}/Nu_{SC} for staggered rows I and II at S_x/D=1.6, S_y/D=2.5 and S_x/D=2.5, S_y/D=1.6 almost agree with the corresponding values for in-line rows, as shown in

Figures 15 and 16. It is expected from this comparison that natural convection heat transfer for the rod bundles with the same values of S_x/D and S_y/D does not depend on the bundle geometry.

< Figure 14, 15 and 16 >

3.4 Effect of S_x/D and S_y/D on Heat Transfer

Natural convection heat transfer for the bundle geometry of in-line rows in a 5×5 array was numerically analyzed to examine the effect of S_x/D and S_y/D on heat transfer, at the constant heat flux conditions of R_f=6.78 and 14.2 (q=1×10^6, 2×10^6 W/m^2) for S_x/D and S_y/D ranging from 1.6 to 2.5.

3.4.1 Effect of S_x/D

The theoretical values of Nu_{av}/Nu_{SC} are plotted on Nu_{av}/Nu_{SC} versus S_x/D graph in **Figure 17**. The Nu_{av}/Nu_{SC} value for R_f=6.78 and S_y/D=1.6 is 68 % of that for a single cylinder at S_x/D=1.8, becomes higher with the increase in S_x/D and is 80 % at S_x/D=2.5. The Nu_{av} becomes 21 % larger with the increase in S_x/D from 1.8 to 2.5. The values of Nu_{av}/Nu_{SC} for R_f=14.2 and S_y/D=1.6 show nearly the same trend of dependence on S_x/D, although they are almost 9 % higher than the corresponding values for R_f=6.78 and S_y/D=1.6. The values of Nu_{av}/Nu_{SC} for R_f=6.78 and 14.2, and S_y/D=2 almost agree with the corresponding values for S_y/D=1.6, although they are slightly higher than the latter.

< Figure 17 >

3.4.2 Effect of S_y/D

The Nu_{av}/Nu_{SC} values are shown versus S_y/D in **Figure 18**. The Nu_{av}/Nu_{SC} value for R_f=6.78 is 63 % of that for a single cylinder at S_y/D=1.8, becomes higher for the higher value of S_y/D and is 66 % at S_y/D=2.5. The average Nusselt number becomes 5 % larger with the increase in S_y/D from 1.8 to 2.5. The values of Nu_{av}/Nu_{SC} for R_f=14.2 show nearly the same

trend of dependence on S_y/D and are almost 9 % higher than the corresponding values for R_f=6.78 as mentioned above.

The values of Nu_{av} become higher with the increase in the values of S_x/D and S_y/D. It should be noted that natural convection heat transfer from a horizontal rod bundle is far more influenced by the distance between the center axes on the column, S_x, than be done by that on the row, S_y. It is considered from this fact that the optimum combination of S_x/D and S_y/D may exist under the condition of a constant value of $S_x/D \times S_y/D$.

< Figure 18 >

3.5 Effect of S_x/S_y with the Same Rod Density on Heat Transfer

The higher Nu_{av} under the condition of $S_x/D \times S_y/D$=4 was examined by changing the ratio of S_x/D to S_y/D. The values of the average Nusselt number, Nu, for the bundle geometry of in-line rows in 5×5 and 7×7 arrays are numerically analyzed for two ratios of S_x to S_y at R_f ranging from 0.128 to 14.2 (q=2×10^4~2×10^6 W/m^2) ; S_x/S_y=1.6/2.5 and S_x/S_y=2.5/1.6. The values of Nu_{av}/Nu_{SC} for S_x/D=1.6, S_y/D=2.5 and S_x/D=2.5, S_y/D=1.6 are plotted in **Figures 9, 12 and 13** with those for S_x/D=2, S_y/D=2. The values of Nu_{av}/Nu_{SC} for S_x/D=2.5, S_y/D=1.6 are almost 10 % higher than those for S_x/D=2, S_y/D=2 for the whole range of R_f numerically analyzed here and the values of Nu_{av}/Nu_{SC} for S_x/D=1.6, S_y/D=2.5 are almost 10 % lower than those for S_x/D=2, S_y/D=2.

The theoretical values of Nu_{av}/Nu_{SC} for the bundle geometry of in-line rows in a 5×5 array are shown versus S_x/S_y in **Figure 19** with R_f as a parameter. As shown in the figure, the Nu_{av}/Nu_{SC} value at S_x/S_y=1.6/2.5 for R_f=4.67 are 63 % of that for a single cylinder, that at S_x/S_y=2/2 are 70 % and that at S_x/S_y=2.5/1.6 are 76 %. The Nu_{av}/Nu_{SC} value becomes 20 % higher with the increase in S_x/S_y from 1.6/2.5 to 2.5/1.6. The values of Nu_{av}/Nu_{SC} for R_f=6.78 and 14.2 show nearly the same trends of dependence on S_x/S_y, although they are far higher than the corresponding values for R_f=4.67. The theoretical values of Nu_{av}/Nu_{SC} for the bundle

geometry of in-line rows in a 7×7 array are shown in **Figure 20** and those for staggered rows I and II in 5×5, 5(6)×5 arrays are shown in **Figures 21 and 22**, respectively. The trends of dependence of Nu/Nu_{SC} on S_x/S_y are almost in agreement with that in **Figure 19**. It is suggested that the higher heat transfer from a horizontal rod bundle will be realized for the bundle geometry whose value of S_x/D is larger than that of S_y/D under the condition of $S_x/D \times S_y/D$=constant.

< Figure 19, 20, 21 and 22 >

4. Correlation for Horizontal Rod Bundles of In-Line Rows, Staggered Rows I and II with Various S_x/S_y

It was recognized that the theoretical values of Nu_{av} for rod bundles do not depend on the bundle geometry and become higher for higher value of S_x/S_y. A correlation for Nu_{av} from horizontal rod bundle of in-line rows, staggered rows I and II with various S_x/S_y was given as follows based on Equation (14) and the calculated results for the values of S_x/S_y other than unity.

$$Nu_{av} / Nu_{SC} = [1.77(Nu_{SB})_{av} / Nu_{SC} - 0.871 / (N_{xm} \times N_{ym})^{1/4}](S_x / S_y)^{1/4} \qquad (15)$$

In the case of $S_x/S_y \neq 1$, the $(Nu_{SB})_{av}/Nu_{SC}$ value can be calculated from Equation (10) by introducing an effective value S_{eff} given by $S_{eff}=(S_x \times S_y)^{1/2}$ instead of S, and Nu_{SC} value from Equation (7). The curves of Nu_{av}/Nu_{SC} for each value of R_f derived from this correlation are shown as an individual curve for comparison in **Figures 9 and 12 to 22**. As shown in these figures, the correlation can describe the theoretical solutions of Nu_{av} for the bundle geometry of in-line rows, staggered rows I and II in 5×5, 5(6)×5, 7×7 and 9×9 arrays for S_x/D and S_y/D ranging from 1.6 to 2.5 within 10 % difference.

It is expected from these comparisons that this correlation can be used for the design and the safety evaluation of a heat exchanger for a sodium cooled fast breeder reactor in the region of low Grashof numbers, $Gr \leq 10^8$. However, rod diameter of a heat exchanger for a

power plant may be 3 or 4 times larger than that used in this work, D=7.6 mm. In such a case, the values of Gr become larger than 10^8 in higher heat flux range of this analysis. Turbulence effects may play an important role on heat transfer for rod arrays at $Gr>10^8$ [18]. The study of rod arrays for higher Grashof numbers will appear in the near future.

5. Summary and Conclusions

Natural convection heat transfer from horizontal rod bundles for three types of the bundle geometry of in-line rows, staggered rows I and II in 5×5, 5(6)×5, 7×7, 9×9 arrays with S_x/D and S_y/D ranging from 1.6 to 2.5 was numerically analyzed in liquid sodium.

The spatial distribution of average Nusselt numbers, Nu, which is symmetrical with respect to the y axis are clarified. The values of Nu for each column become smaller with the increase in the row number. The value of Nu at the center rod for the lowest row is the maximum and the Nu value at the center rod for the uppermost row is the minimum. The values of Nu for the edge column are higher than those for other column on the same row number except those for the lowest row.

The average Nusselt number for a rod bundle, Nu_{av}, becomes lower with the decrease in the value of R_f and higher with the increase in the value of S_x/D and S_y/D.

The values of Nu_{av} on various bundle geometries with the same values of S_x/D and S_y/D are almost in agreement independent of the bundle geometry.

The higher Nu_{av} value under the condition of $S_x/D×S_y/D$=4 was examined by changing S_x/D from 1.6 to 2.5. They are higher for the larger value of S_x/D. It is suggested that the higher heat transfer from a horizontal rod bundle will be realized for the bundle geometries with higher values of S_x/S_y under the condition of $S_x/D×S_y/D$=constant.

A generalized correlation for Nu_{av} including the effects of S_x/D and S_y/D for various types of bundle geometry was developed. The correlation can describe the theoretical values of Nu_{av} for three types of the bundle geometry of in-line rows, staggered rows I and II in 5×5,

5(6)×5, 7×7, 9×9 arrays with S_x/D and S_y/D ranging from 1.6 to 2.5 within 10 % difference.

Nomenclature

A	= non-dimensional quantity in Equation (8)	
C	= non-dimensional quantity in Equation (9)	
c_p	= isobaric specific heat, J/kg K	
D	= rod diameter, m	
Gr^*	$= \gamma \beta q D^4 / \lambda v^2$, Grashof number for constant heat flux	
g	= acceleration of gravity, m/s^2	
K	= non-dimensional quantity in Eqution (9)	
m	= exponent in Equation (8)	
N	= cylinder number	
N_m	= total number of cylinder	
N_x	= column number	
N_{xm}	= total number of rod in a column	
N_y	= row number	
N_{ym}	= total number of rod in a row	
Nu	= Nusselt number	
Nu_{av}	= average Nusselt number for a rod bundle	
Nu_{CC}	= average Nusselt number for rods of a center column	
Nu_{SB}	= average Nusselt number for rods of single vertical array	
Nu_{SC}	= Nusselt number for single cylinder	
n	= exponent in Equation (9)	
P	= pressure, N/m^2	
Pr	= Prandtl number	
q	= heat flux, W/m^2	

Ra $= Gr\,Pr$, Rayleigh number

Ra^* $= Gr^*Pr$, Rayleigh number for constant heat flux

Ra_d^* $= Gr_d^*Pr$, modified Rayleigh number

R_f $= Gr^*Pr^2/(4+9Pr^{1/2}+10Pr)$, modified Rayleigh number

r radius of a cylinder, m

$(\Delta r)_{out}$ outer control volume width for r-component, m

S = distance between the center axis of two parallel horizontal cylinders, m

S_{eff} $= (S_x \times S_y)^{1/2}$, effective distance, m

S_x = distance between the center axes on abscissa, m

S_y = distance between the center axes on ordinate, m

T = temperature, K

T_0 = bulk liquid temperature, K

TEM analyzed liquid temperature of the outer control volume, K

T_f liquid temperature, K

T_S heater surface temperature, K

t = time, s

u, v = velocity components in x and y directions, m/s

x, y = Cartesian coordinates, m

Greek Symbols

γ = setting angle of the two horizontal cylinders, deg

θ = peripheral angle from the bottom of the cylinder, deg

λ = thermal conductivity, W/(m K)

ν = kinematic viscosity, m^2/s

ρ = density, kg/m^3

τ = viscous stress tensor, kg/s^2 m

References

[1] Marsters GF, Arrays of Heated Horizontal Cylinders in Natural Convection. Int. J. Heat Mass Transfer. 1972; 15: 921-933.

[2] Lieberman J, Gebhard B, Interactions in Natural Convection from an Array of Heated Elements, Experimental. Int. J. Heat and Mass Transfer. 1968; 12-11: 1387-1396.

[3] Warrington RO, Weaver RA, Natural Convection Heat Transfer between Arrays of Horizontal Cylinders and Their Enclosures. Heat Transfer in Enclosures, ASME HTD Vol. 39. 1984.

[4] Fedorovitch ED, The Thermal Conditions and the Strength of a Spent Fuel Package: Analysis and Test. Proceedings of the 9th International Symposium on the Packaging and Transportation of Radioactive Materials, CONF-890631-Vol. 3. 1989: 1647-1668.

[5] Irino M, Oohashi M, Irie T., Nishikawa T, Study on Surface Temperatures of Fuel Pins in Spent Nuclear Fuel Dry Shipping/Storage Casks. Proceedings of an International Symposium on the Packing and Transportation of Radioactive Materials, Davos, Vol. 2, 1986: 585-589.

[6] Vdovets NV, Grivnin AI, Gotovskii MA, Pervitskaya TA, Fromzel VN, Fedorovitch ED, Shleifer VA, Natural-Convection Heat Transfer in Horizontal Bundles of Fuel Rods. High Temperature, A Translation of Teplofizika Vysokikh Temperatur. 1987; 24-4: 545-552.

[7] Keyhani M, Luo L, A Numerical Study of Convection Heat Transfer within Enclosed Horizontal Rod-Bundles. Journal of Nuclear Science and Engineering, 1995; 119-2, 116-127.

[8] Keyhani M, Dalton TE, An Experimental Study of Convection Heat Transfer within Enclosed Horizontal Rod-Bundles. International Mechanical Engineering Congress and Exposition-Proceedings of the ASME Heat Transfer Division, ASME Publication HTD-Vol. 317-2, 1995: 235-245.

[9] Patankar SV, Numerical Heat Transfer and Fluid Flow. Hemisphere Pub. Corp.: New York; 1980.

[10] Hata K, Shiotsu M, Takeuchi Y, Sakurai A, Natural convection heat transfer on two horizontal cylinders in liquid sodium. Proceedings of the 7th International Meeting on Nuclear Reactor Thermal-Hydraulics, Vol. 2. 1995: 1333-1350.

[11] Hata K, Shiotsu M, Takeuchi Y, Sakurai A, Natural convection heat transfer from two parallel horizontal cylinders in liquid sodium. International Mechanical Engineering Congress and Exposition-Proceedings of the ASME Heat Transfer Division, ASME Publication HTD-Vol. 317-1. 1995: 245-257.

[12] Hata K, Shiotsu M, Takeuchi Y, Hama K, Sakurai A, Sagayama Y, Natural convection heat transfer from horizontal rod bundles in liquid sodium. Proceedings of Eighth International Topical Meeting on Nuclear Reactor Thermal Hydraulics, Vol. 2. 1997: 817-827.

[13] Hata K, Takeuchi Y, Hama K, Shiotsu M, Shirai Y, Fukuda K, Natural convection heat transfer from a vertical cylinder in liquid sodium. Proceedings of the 7th International Conference on Nuclear Engineering (ICONE-7), Paper No. ICONE-7122. 1999: 1-10.

[14] Hata K, Takeuchi Y, Shiotsu M, Sakurai A, Natural convection heat transfer from a horizontal cylinder in liquid sodium (Part 2: Generalized correlation for laminar natural convection heat transfer). Nuclear Engineering and Design, 1999c; 194, 185-196.

[15] Michel Favre-Marinet, Sedat, Tardu, Convective Heat Transfer. ISTE Ltd and John Wiley & Sons, Inc.: Great Britain and United States; 2009.

[16] Hanjalic K, Kenjeres S, Tummers MJ, Jonker HJJ, Analysis and Modeling of Physical

Transport Phenomena. Published by VSSD: The Netherlands; 2009.

[17] Spalding DB, The PHOENICS Beginner's Guide. Pub. by CHAM: UK; 1991,.

[18] Borishanski VM, et al., Jydkometallicheskie Tepronositeli (Liquid Metal Heating Medium). Atomizdat: Moscow; 1967.

List of figure captions

23

Table 1.   Parameters for Calculation

Horizontal Rod Bundles

System Pressure	101.3 kPa
Diameter of Rod (D)	7.6 mm
Outer Control Volume Width for r-component ($(\Delta r)_{out}$)	0.4 mm
Array Size ($N_{x_m} \times N_{y_m}$)	5 × 5, 5(6) × 5, 7 × 7, 9 × 9
Bundle Geometry	In-line Rows, Staggered Rows I, Staggered Rows II
S_x/D, S_y/D (S=Rod Pitch)	1.6, 1.8, 2, 2.2, 2.4, 2.5
Liquid Temperature	673 K
Heat Flux (q)	1×10^4, 2×10^4, 7×10^4,
	2×10^5, 7×10^5, 1×10^6,
	2×10^6, 7×10^6 W/m^2
Gr^*	1.20×10^4, 2.41×10^4, 8.54×10^4,
	2.49×10^5, 9.33×10^5, 1.38×10^6,
	3.06×10^6, 1.43×10^7
$Ra^*(=Gr^*Pr)$	5.98×10 , 1.20×10^2, 4.24×10^2,
	1.23×10^3, 4.50×10^3, 6.59×10^3,
	1.42×10^4, 6.17×10^4
$R_f(=Gr^*Pr^2/(4+9Pr^{1/2}+10Pr))$	0.0637, 0.128, 0.449,
	1.29, 4.67, 6.78,
	14.2, 63.1
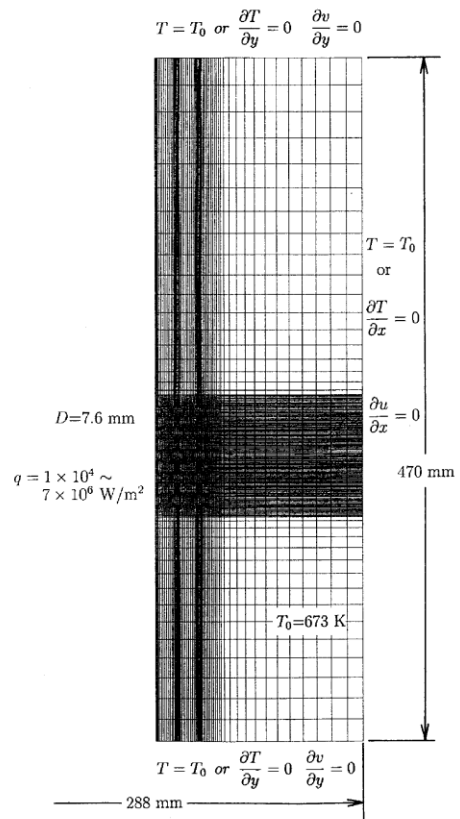
Figure 1 (a).   Boundary fitted coordinates for a 5×5 array.
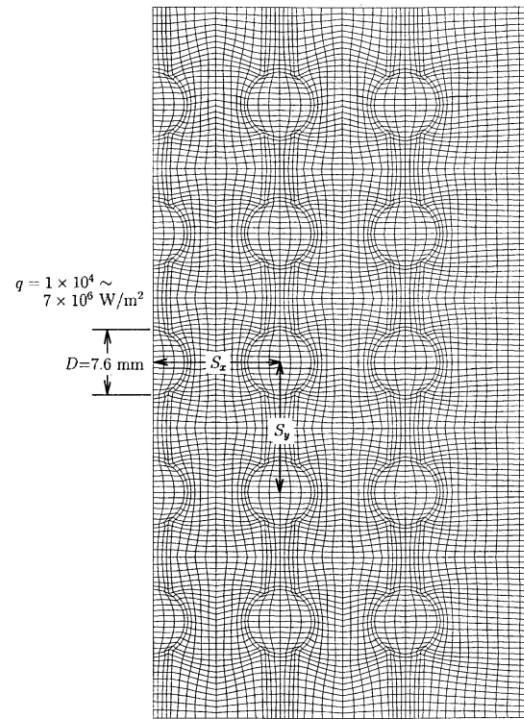
Figure 1 (b). Details of boundary fitted coordinates for a 5×5 array.
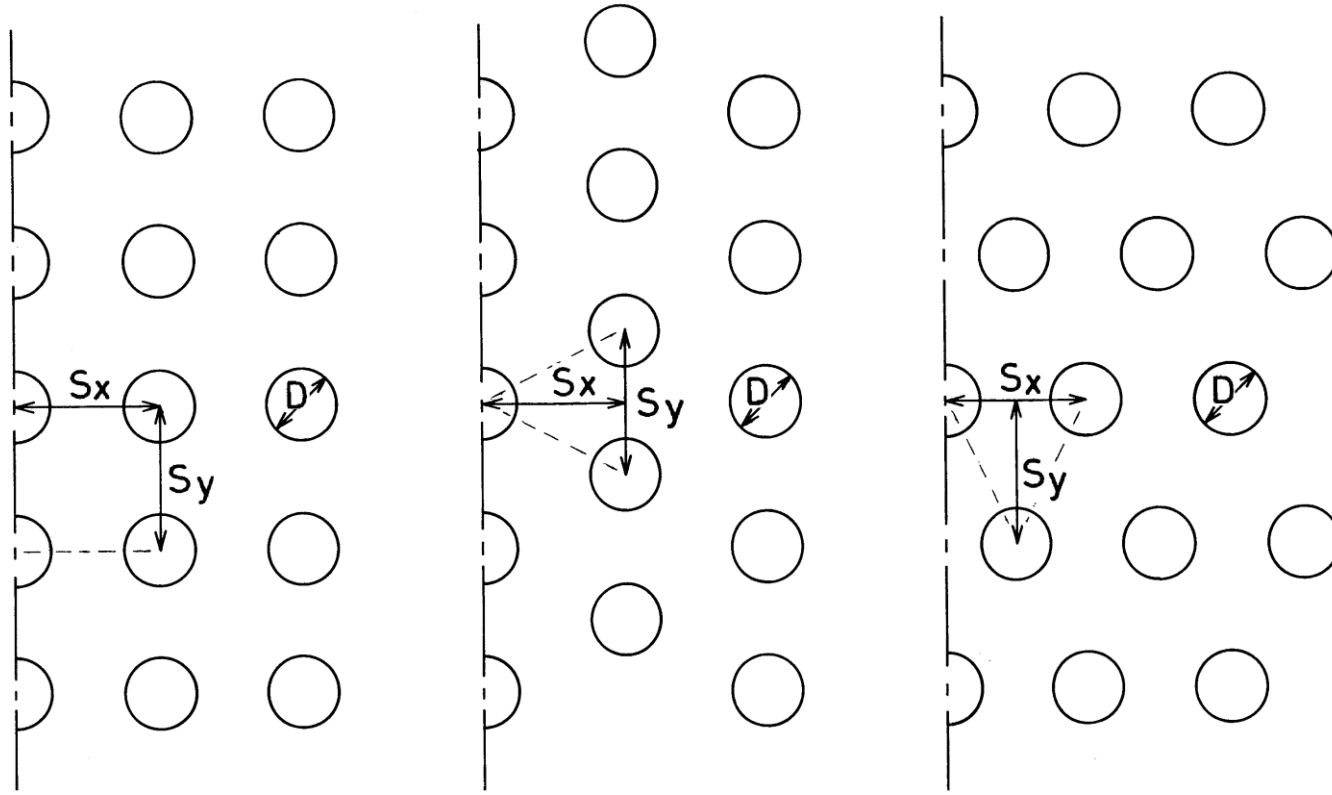
Figure 2.   Bundle geometry: (a) In-line rows (IR); (b) Staggered rows I (SRI); (c) Staggered rows II (SRII).
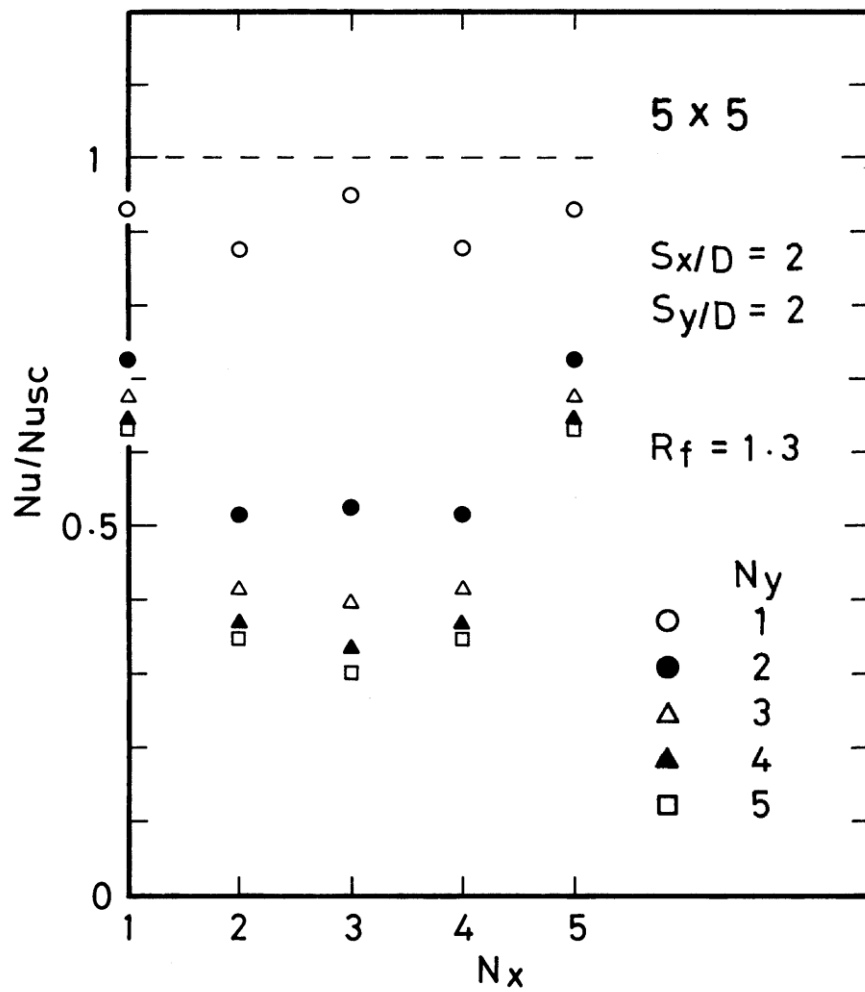
Figure 3.   *Nu/Nu$_{SC}$* versus *N$_x$* for a 5×5 array with *N$_y$* as a parameter at *R$_f$*=1.30.
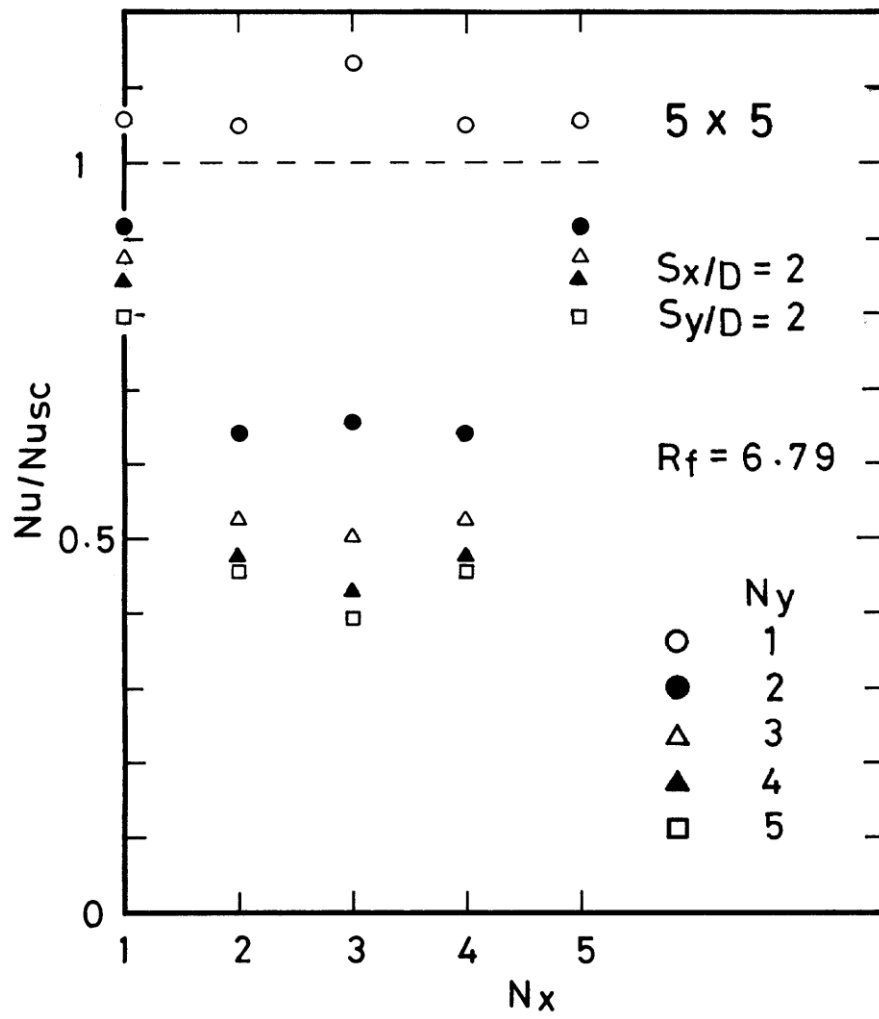
Figure 4.   *Nu/Nu$_{SC}$* versus *N$_x$* for a 5×5 array with *N$_y$* as a parameter at *R$_f$*=6.79.

28

Figure 5. Contour of liquid temperature for a 5×5 array at R_f=6.79.

Velocity, m/s

	38.16374
	35.77905
	33.39436
	31.00967
	28.62497
	26.24028
	23.85559
	21.47090
	19.08621
	16.70151
	14.31682
	11.93213
	9.547438
	7.162745
	4.778053
	2.393361
	0.008669
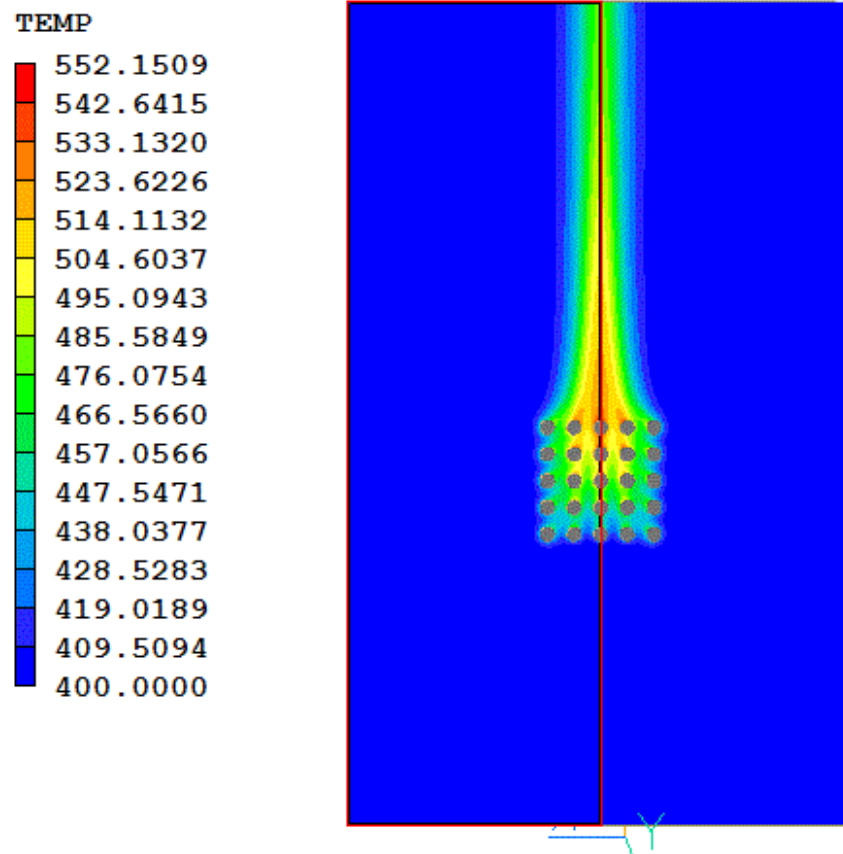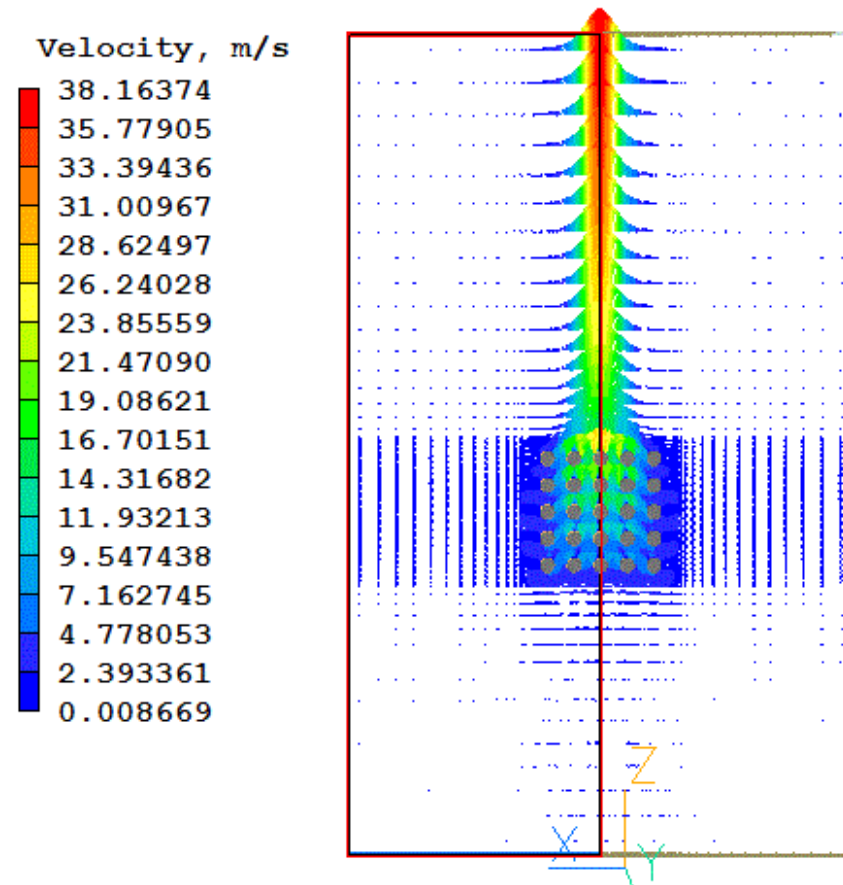
Natural Convection from 5x5 H-Rod Bundle

Figure 6.   Distribution of velocity vectors for a 5×5 array at R_f=6.79.
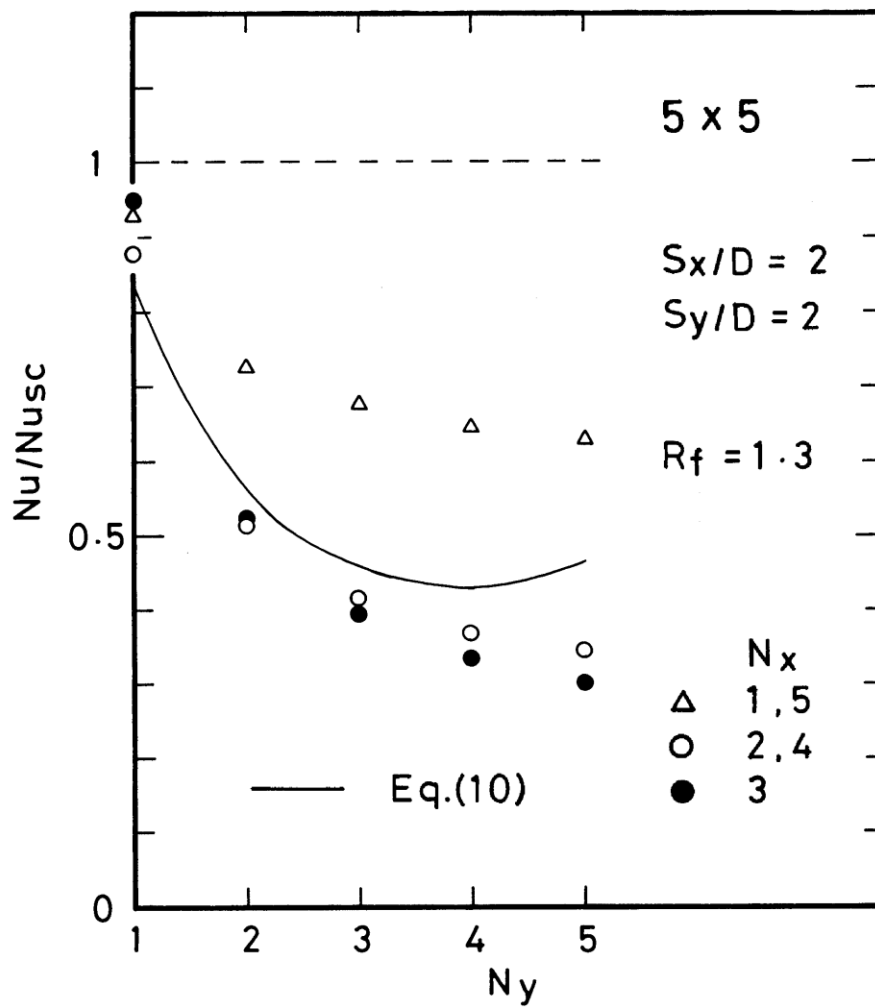
Figure 7. Nu/Nu_{SC} versus N_y for a 5×5 array with N_x as a parameter at R_f=1.30.
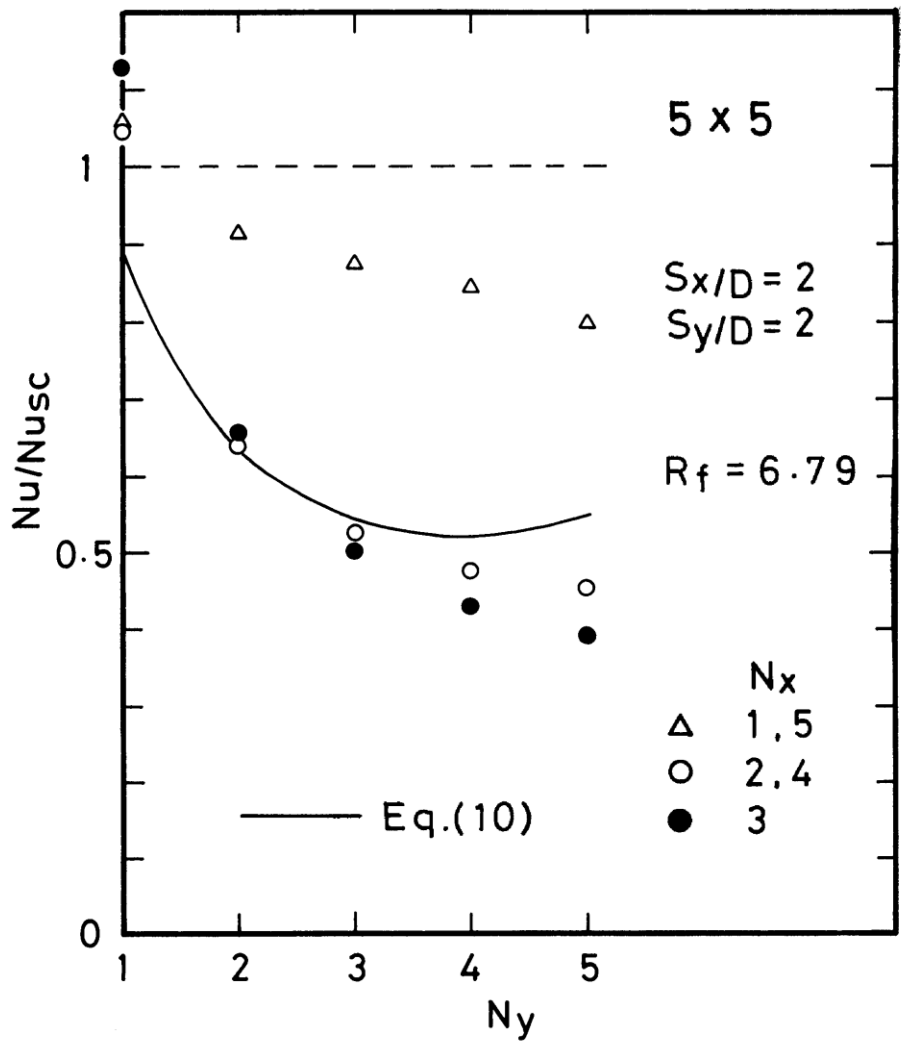
Figure 8. *Nu/Nu$_{SC}$* versus N_y for a 5×5 array with N_x as a parameter at R_f=6.79.
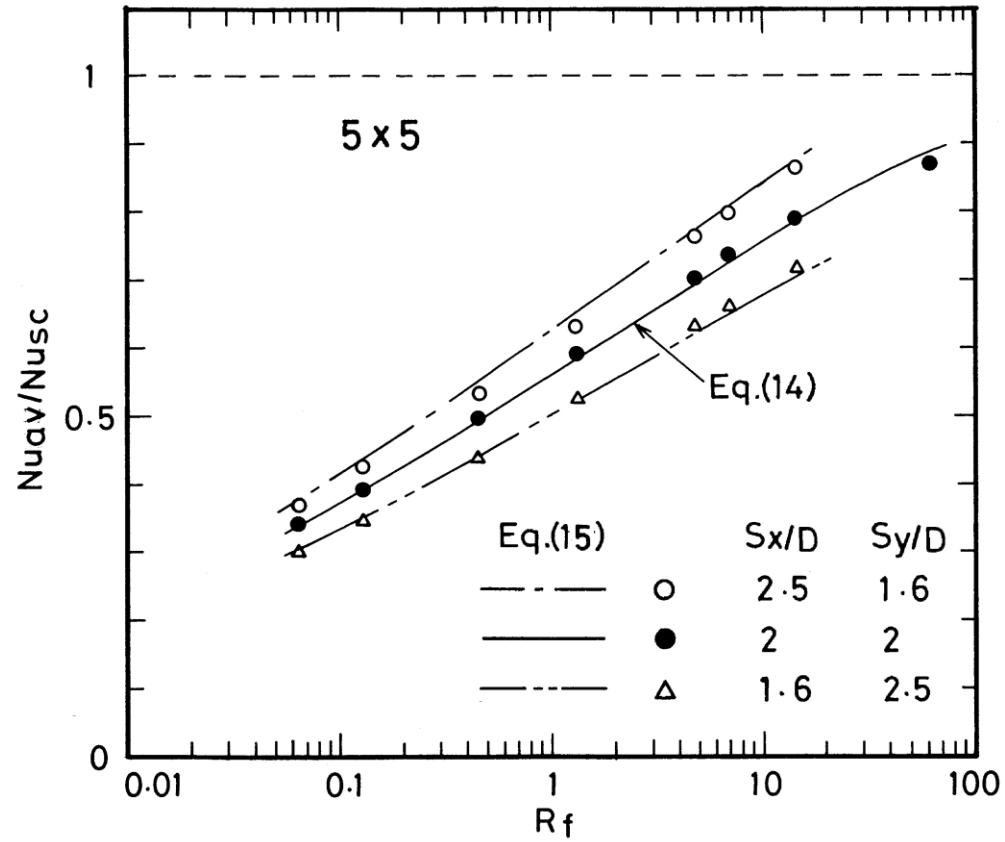
Figure 9. Nu_{av}/Nu_{SC} versus R_f for a 5×5 array with S_x/D and S_y/D as a parameter. Comparison with the predicted curves, Equations (14) and (15).
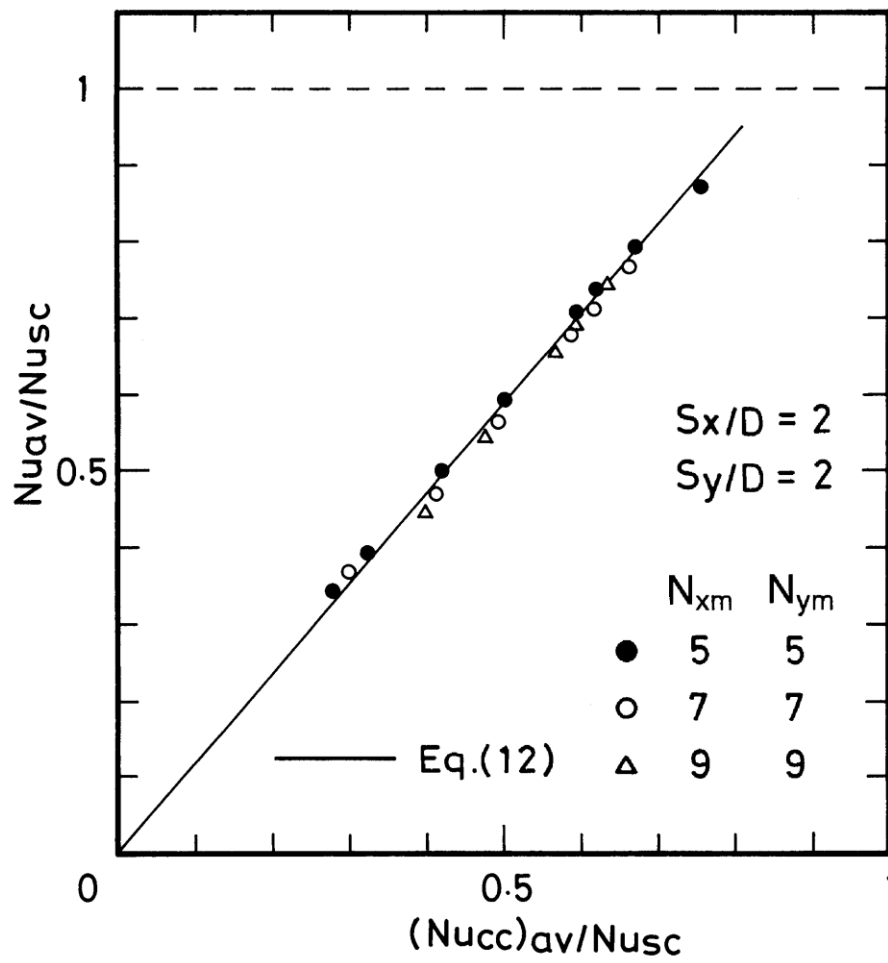
Figure10. Nu_{av}/Nu_{SC} versus $(Nu_{CC})_{av}/Nu_{SC}$ for 5×5, 7×7 and 9×9 arrays. Comparison with the predicted curve, Equation (12).
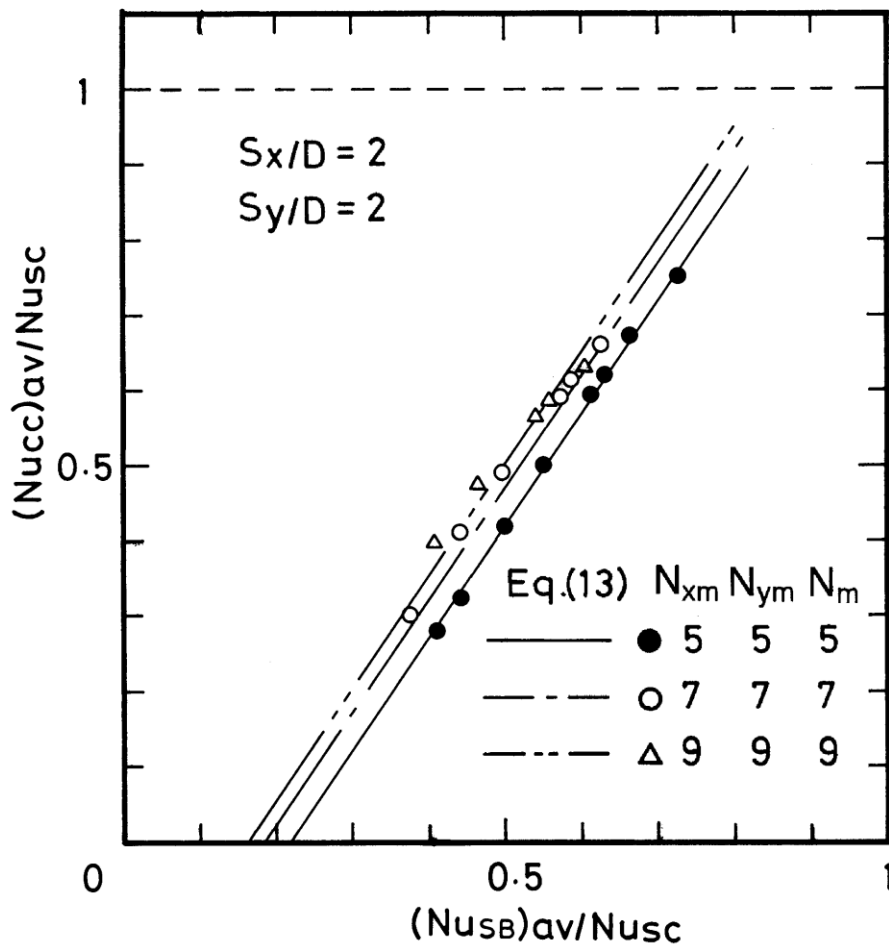
Figure 11. $(Nu_{CC})_{av}/Nu_{SC}$ versus $(Nu_{SB})_{av}/Nu_{SC}$ for 5×5, 7×7 and 9×9 arrays. Comparison with the predicted curve, Equation (13).
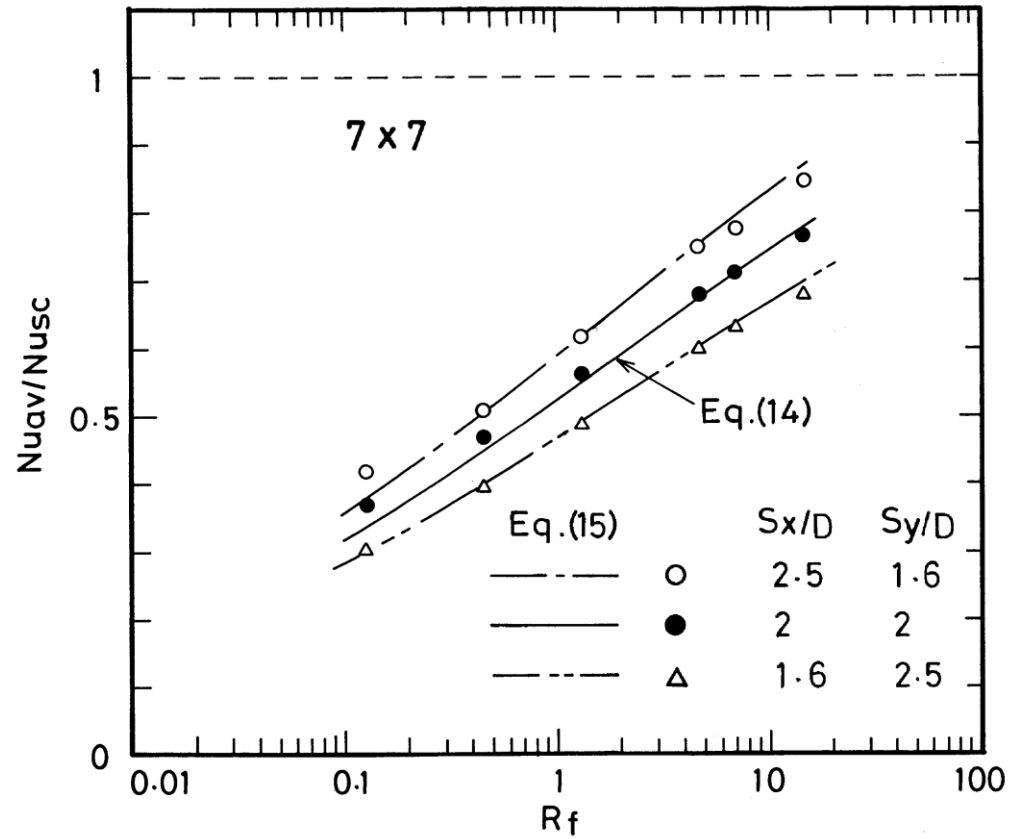
Figure 12. Nu_{av}/Nu_{SC} versus R_f for a 7×7 array with S_x/D and S_y/D as a parameter. Comparison with the predicted curves, Equations (14) and (15).
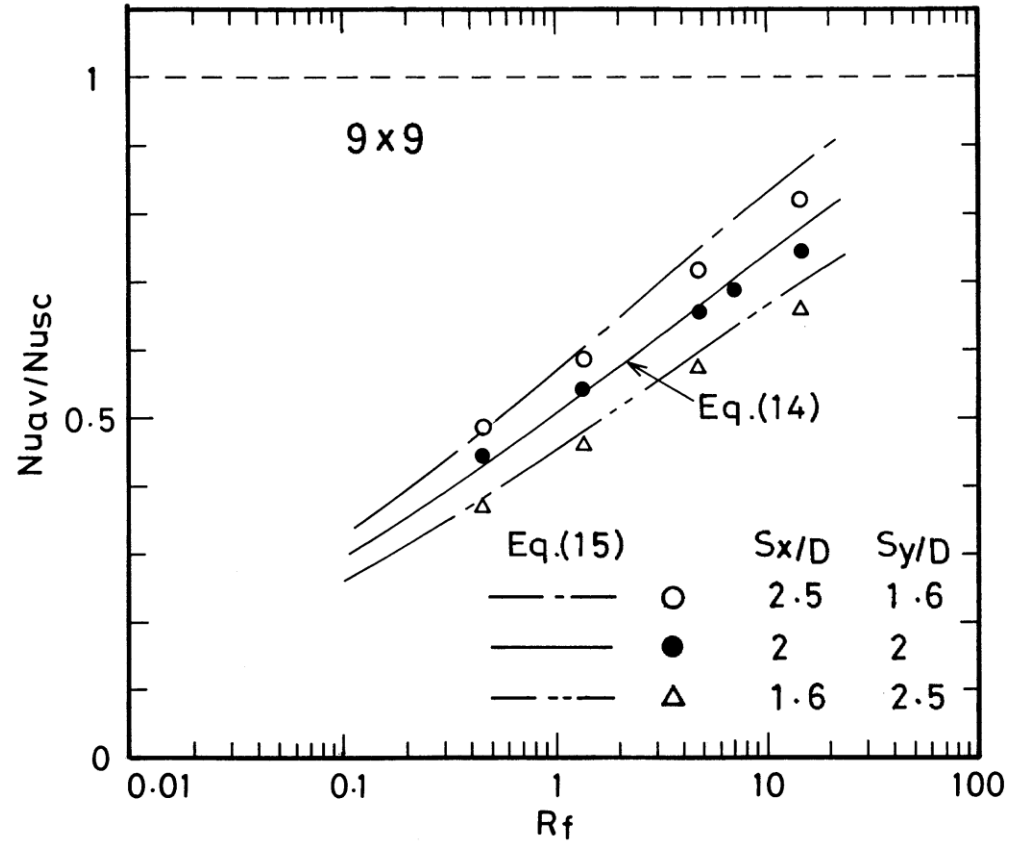
Figure 13.　　Nu_{av}/Nu_{SC} versus R_f for a 9×9 array with S_x/D and S_y/D as a parameter. Comparison with the predicted curves, Equations (14) and (15).
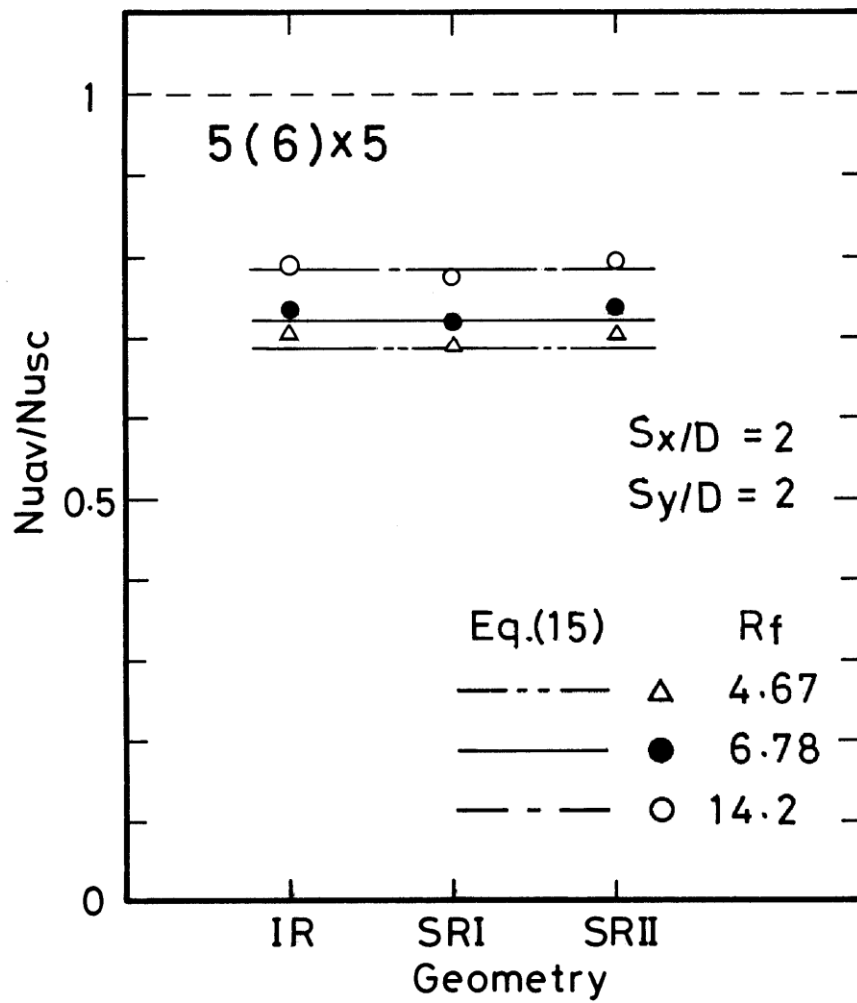
Figure 14. Nu_{av}/Nu_{SC} versus bundle geometry for $S_x/D=S_y/D=2$ with R_f as a parameter.
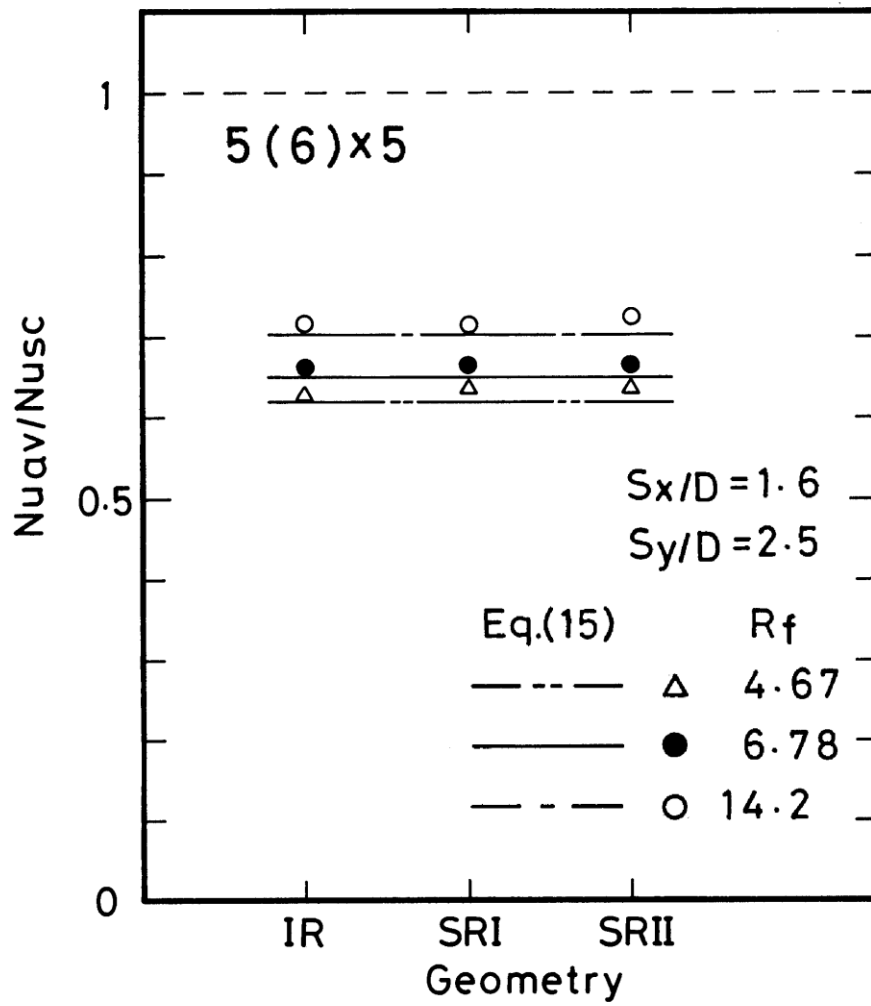
Figure 15. Nu_{av}/Nu_{SC} versus bundle geometry for S_x/D=1.6, S_y/D=2.5 with R_f as a parameter.
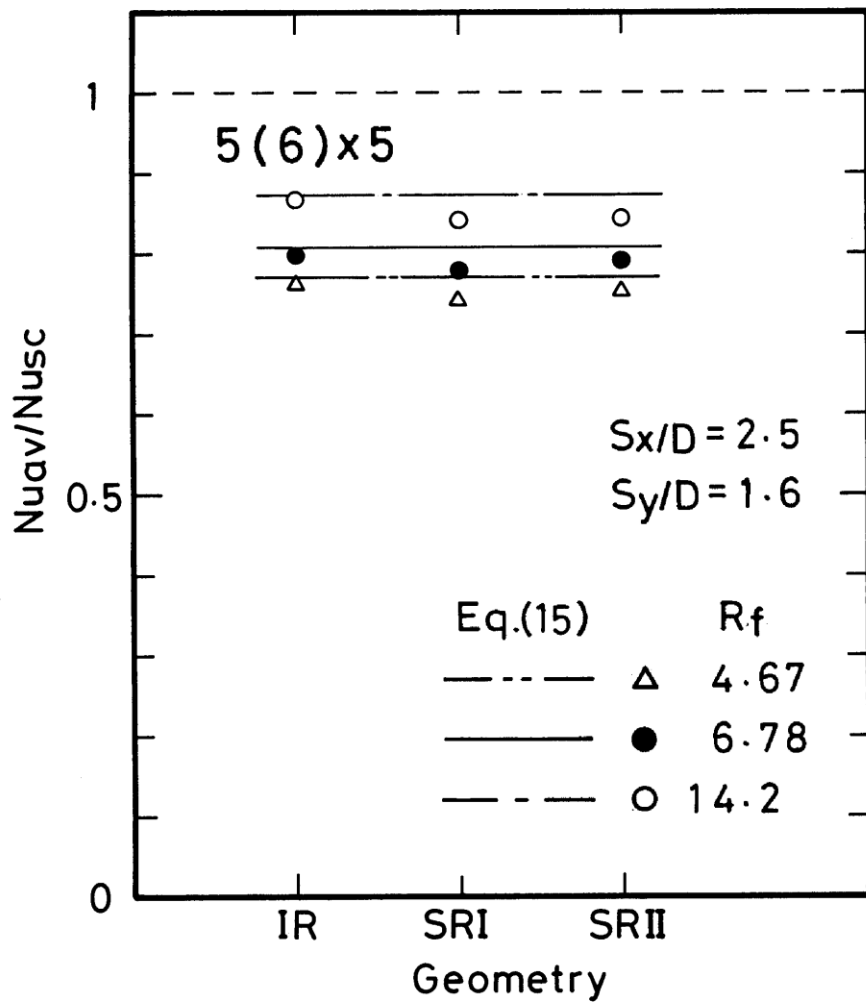
Figure 16. Nu_{av}/Nu_{SC} versus bundle geometry for S_x/D=2.5, S_y/D=1.6 with R_f as a parameter.
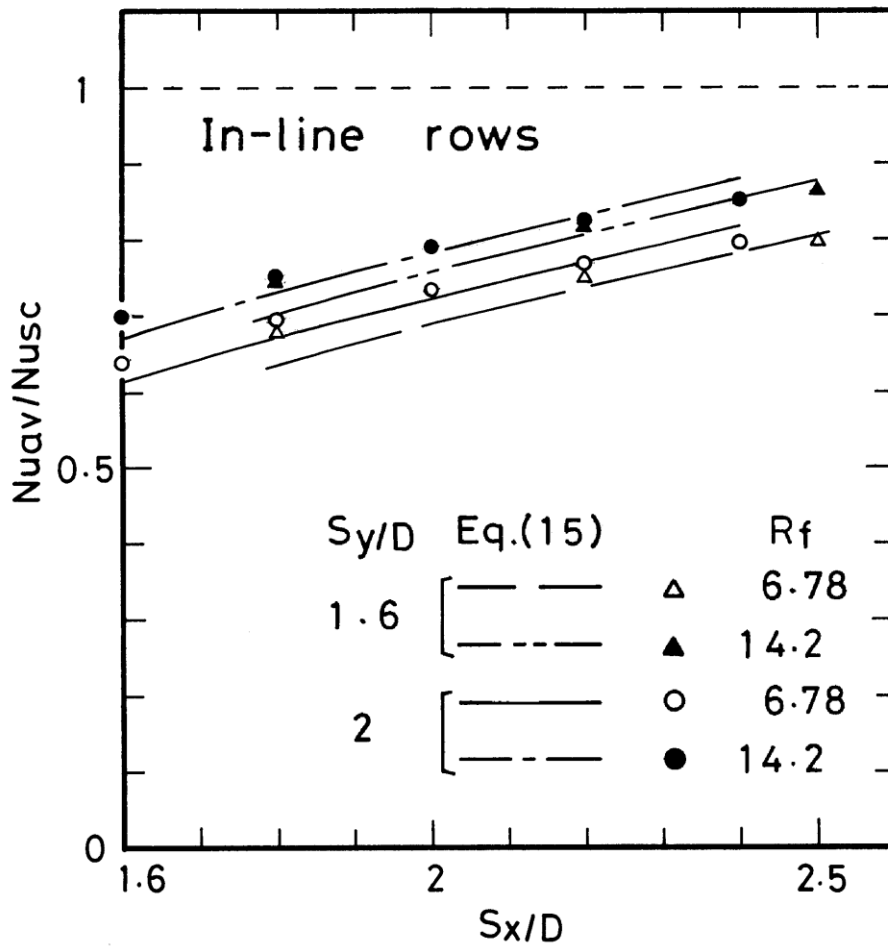
Figure 17. Nu_{av}/Nu_{SC} versus S_x/D with R_f as a parameter. Comparison with the predicted curve, Equation (15).
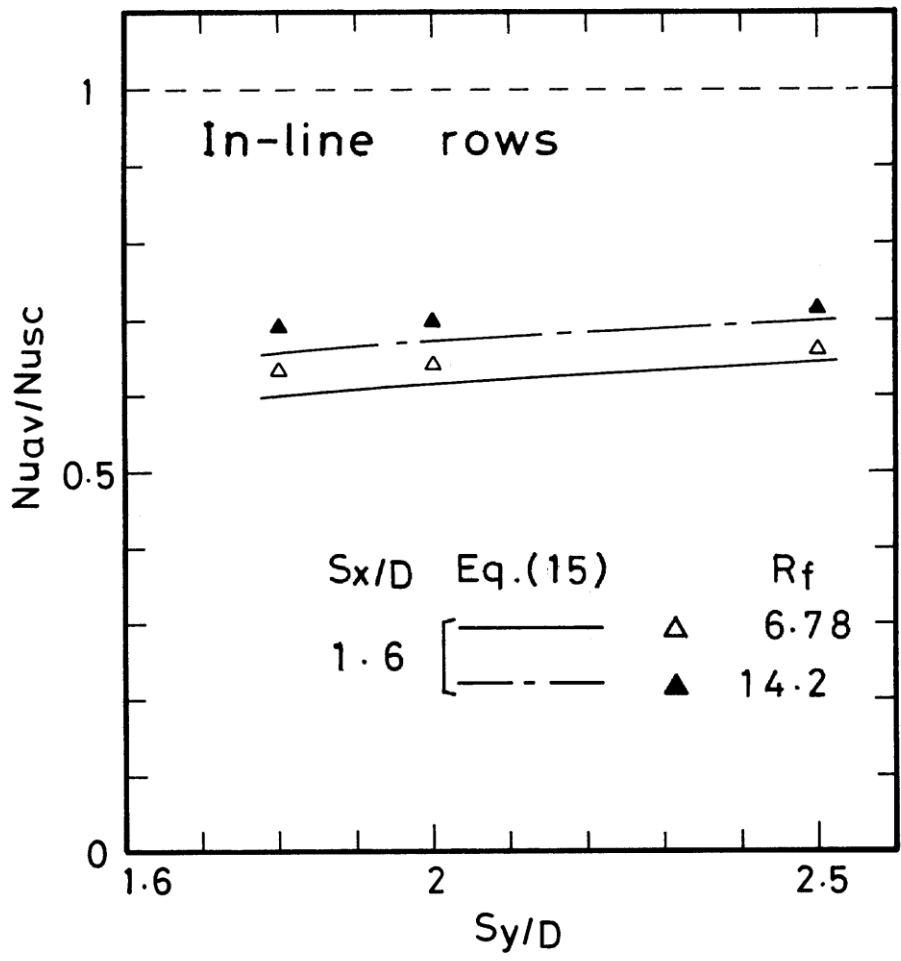
Figure 18. Nu_{av}/Nu_{SC} versus S_y/D with R_f as a parameter. Comparison with the predicted curve, Equation (15).
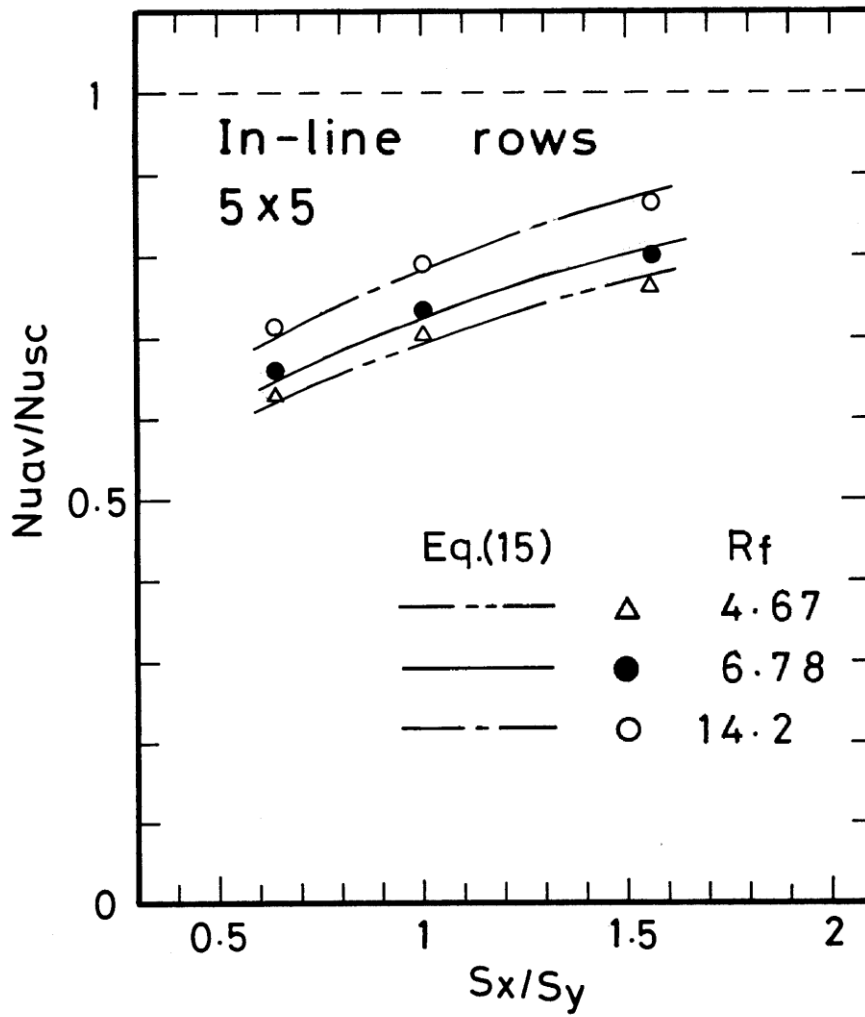
Figure 19. Nu_{av}/Nu_{SC} versus S_x/S_y for in-line rows in a 5×5 array with R_f as a parameter. Comparison with the predicted curve, Equation (15).
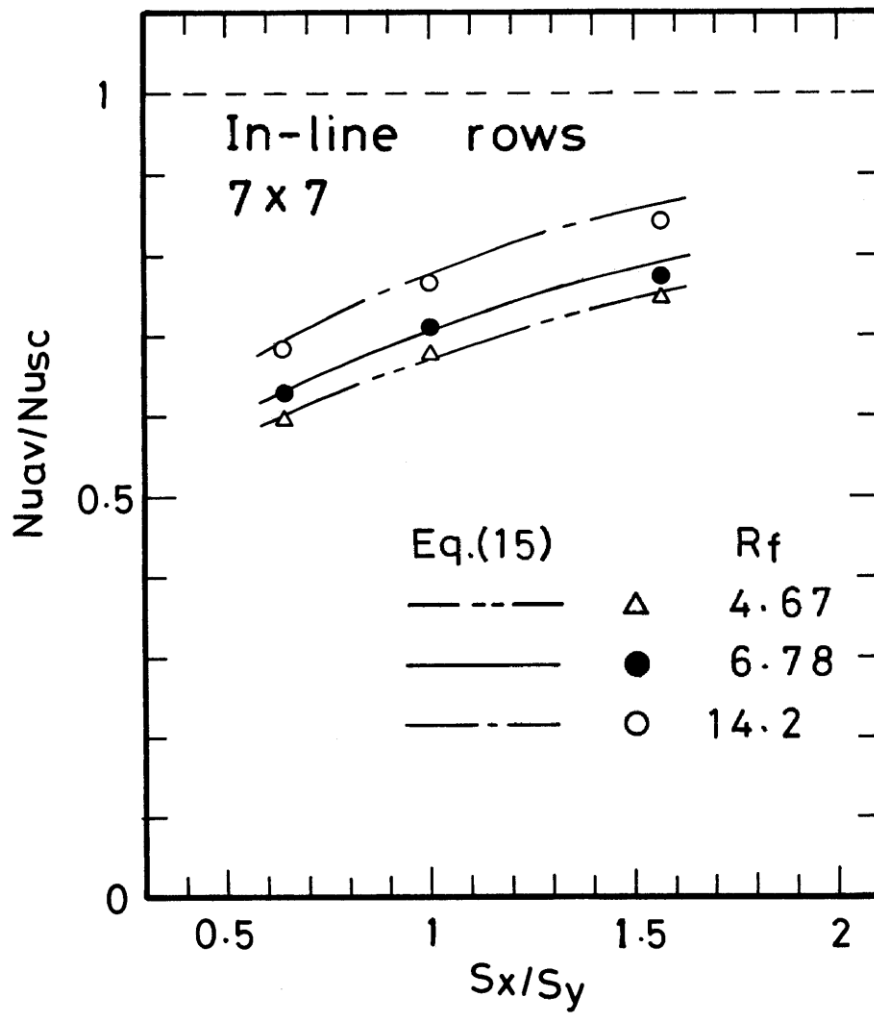
Figure 20. Nu_{av}/Nu_{SC} versus S_x/S_y for in-line rows in a 7×7 array with R_f as a parameter. Comparison with the predicted curve, Equation (15).
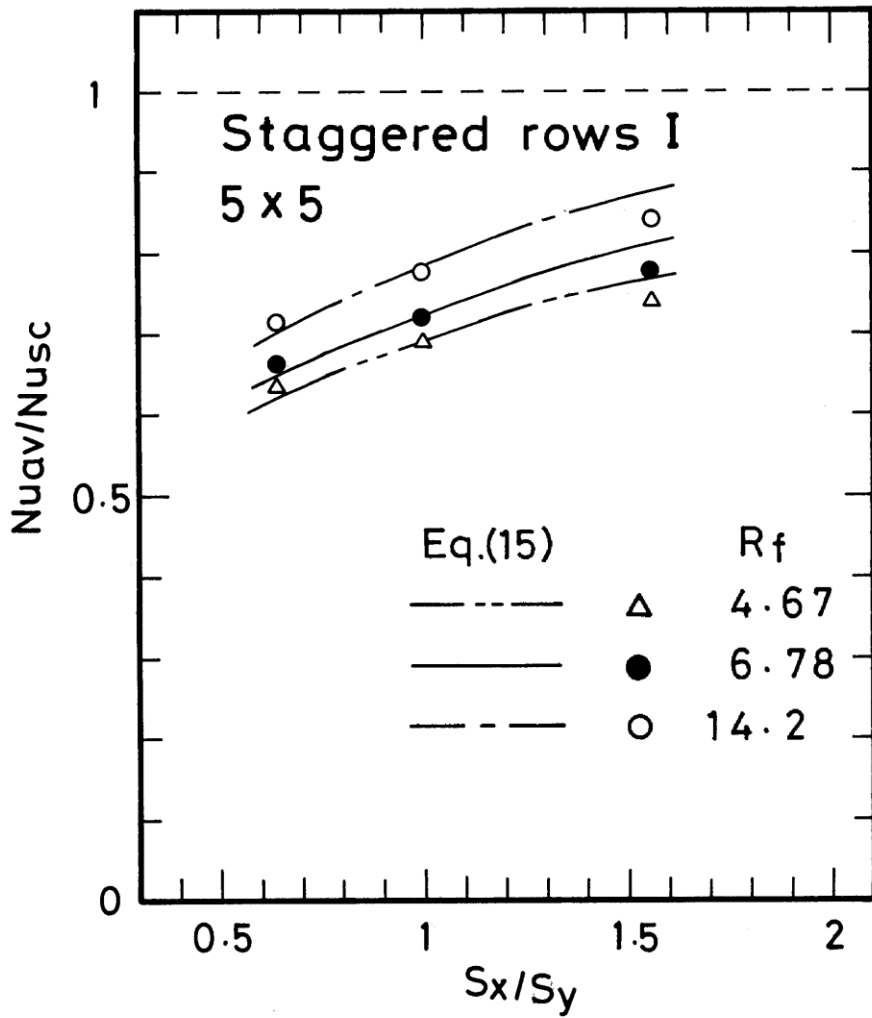
Figure 21.　　　Nu_{av}/Nu_{SC} versus S_x/S_y for staggered rows I in a 5×5 array with R_f as a parameter. Comparison with the predicted curve, Equation (15).
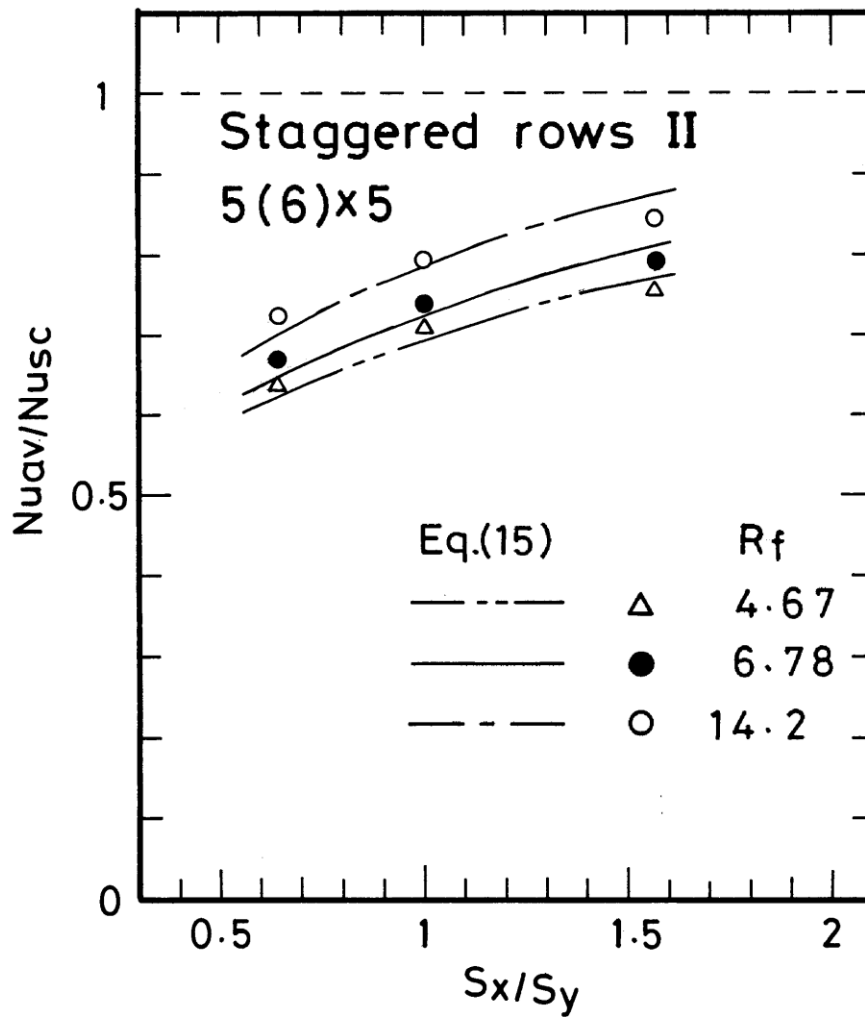
Figure 22. Nu_{av}/Nu_{SC} versus S_x/S_y for staggered rows II in a 5(6)×5 array with R_f as a parameter. Comparison with the predicted curve, Equation (15).